Chinese Journal of Chemical Engineering 94 (2026) 208–222

Contents lists available at ScienceDirect

Chinese Journal of Chemical Engineering

journal homepage: www.elsevier.com/locate/CJChE

Full Length Article

Economic optimization and uncertainty analysis of hydrogen fuel cell in integrated energy systems

Zihan Cheng, Xiaojuan Ma, Yufei Wang *

School of Chemical Engineering and Environment, China University of Petroleum (Beijing), Beijing 102249, China

ARTICLE INFO

Article history:
Received 24 October 2025
Received in revised form
1 January 2026
Accepted 4 January 2026
Available online 7 February 2026

Keywords:
Hydrogen fuel cell
Hydrogen energy storage
Uncertainty
Carbon emission
Integrated energy system

ABSTRACT

As a key technology for stabilizing renewable energy, hydrogen fuel cells (FC) play a crucial role in enhancing energy utilization efficiency and reducing carbon emissions in the power and chemical industries. Previous studies have examined FC mainly from technical or microgrid perspectives, hydrogen fuel cells (HFC) economic performance and stability contribution in electricity–hydrogen integrated energy systems (EH-IES) under uncertainty remain insufficiently explored. This paper proposes an optimization model for integrated energy systems (IES) with Solid oxide fuel cells (SOFC), aiming at minimizing total annual costs using mixed-integer linear programming (MILP). Based on real-world cases, the sensitivity analysis is carried out to evaluate the impacts of various factors on the economic viability of SOFC, while a robust optimization method is introduced to simulate the uncertainties in energy demand and renewable output. Results show that SOFC becomes economically competitive when the carbon price exceeds 187 CNY·t^{-1} or when the fuel cell capital cost falls below 1676.64 CNY·kW^{-1}. Moreover, SOFC economics improve with increasing electricity and hydrogen demand, while higher thermal and cooling demand reduces their cost-effectiveness. Integrating SOFC reduces total annual cost, cost of carbon emission, and curtailment rates by 0.2%, 7.8%, and 7.1%, respectively. Under high power-hydrogen demand uncertainty, SOFCs mitigate cost increases and enhance system stability. This study provides theoretical underpinnings for SOFC applications in low-carbon energy systems and serves as a reference for IES optimization design.
© 2026 The Chemical Industry and Engineering Society of China, and Chemical Industry Press Co., Ltd. All rights are reserved, including those for text and data mining, AI training, and similar technologies.

1. Introduction

As living standards continue to improve, energy consumption has risen sharply, leading to increasingly severe environmental issues caused by conventional energy sources. This significantly increases the challenges of achieving the goal of carbon neutrality [1]. Globally, only 4.5% of regions have achieved carbon neutrality, while most countries plan to reach this goal between 2050 and 2070 [2]. Energy transition has become a global consensus. In this context, renewable energy, as a substitute for traditional fossil fuels, has gained widespread attention and interest [3]. Solar photovoltaic (PV) [4] and wind turbines (WT) [5] play a key role in the transition to 100% renewable energy due to their relatively low unit capital expenditure (CAPEX) [6]. The advantages of these technologies have led researchers to prioritize them in energy planning [7].

The integration of renewable energy with traditional energy sources is crucial for reducing greenhouse gas emissions and achieving zero carbon emissions [8]. However, renewable energy is intermittent and volatile, making it necessary to rely on energy storage technologies to mitigate energy fluctuations and reduce energy waste [9]. However, many current energy storage technologies have drawbacks such as short lifespan, low energy density, and environmental issues [10]. Therefore, the development of new clean energy conversion and storage technologies remains an urgent global need.

As a fuel that produces only water vapour as a byproduct, hydrogen offers a green and clean energy option, making it a core component of clean and sustainable energy. Its high energy density makes storage and transportation more efficient, thereby enhancing the availability, independence, and security of energy [11]. Building on this, Holladay *et al.* [12] investigated various methods of hydrogen production using renewable resources and fossil fuels, while Forsberg [13] focused on technologies for hydrogen production using nuclear energy and conventional energy systems. Furthermore, hydrogen has enormous potential not

* Corresponding author.
E-mail address: wangyufei@cup.edu.cn (Y. Wang).

https://doi.org/10.1016/j.cjche.2026.01.004
1004-9541/© 2026 The Chemical Industry and Engineering Society of China, and Chemical Industry Press Co., Ltd. All rights are reserved, including those for text and data mining, AI training, and similar technologies.

only in the transportation sector but also in power generation, industry, and chemical engineering, showcasing a wide range of applications [14]. Currently, the most widely used hydrogen storage technology is high-pressure gaseous hydrogen storage, which is characterized by low energy consumption and cost [15]. Compared to pumped storage and electrochemical energy storage, this technology is pollution-free, unaffected by environmental factors, and its high energy density and ease of storage make it an ideal choice for large-scale, long-duration energy storage, providing an effective solution for the large-scale use of renewable energy [16].

The effective utilization of hydrogen energy depends on efficient energy conversion technologies, which are currently mainly realized through hydrogen gas turbines [17] and HFC [18]. Compared with hydrogen internal-combustion engines, FC entail higher capital expenditure; however, their markedly superior environmental profile renders them a more sustainable and future-proof solution for large-scale decarbonization [19]. Among these, HFCs have become one of the most mature hydrogen utilization technologies due to their high energy conversion efficiency, rapid startup, stable operation, and low noise characteristics [20]. SOFCs not only provide electrical energy but also offer combined heat and power (CHP), thereby improving the overall energy utilization efficiency of the system [21]. Because their conversion is not constrained by the Carnot cycle, SOFC-based CHP systems have proven to achieve efficiencies exceeding 90% [22]. Previous studies have shown the accurate and realistic modelling of SOFC [23]. Moreover, integrating FC into renewable energy systems can enhance system stability and reliability while enabling the efficient utilization of clean energy [24]. In early research, Das *et al.* [25] proposed a hybrid energy system integrating WT, PV, and FC, aimed at providing a stable power supply to the system. With advancements in technology, El-Shatter *et al.* [26] Further introduced smart controls and developed an energy system incorporating PV, WT, and FC. Sun *et al.* [27,28] conducted an efficiency analysis and advanced control strategy for grid-connected FC operating under constant-power conditions, and further employed dynamic programming to realize economic-ahead scheduling of a residential micro-scale combined heat-and-power system based on fuel-cell technology. Recently, Li *et al.* [29] proposed an integrated hydrogen–ammonia–methanol multi-carrier energy conversion system based on SOFCs, highlighting the potential of multi-vector energy coupling for efficient hydrogen utilization. This IES, based on FC, offers a technological pathway for achieving carbon neutrality through electric-hydrogen interchangeable energy storage.

Despite the numerous advantages of FC, their high initial CAPEX and operating expenditure (OPEX) still limit their widespread application [30]. Currently, the economic feasibility of FC in IES remains a topic of debate. Researchers are working to explore under which FCs can yield economic benefits within systems and optimize their application strategies. Nelson *et al.* [31] conducted an economic assessment of a WT/PV/FC hybrid power generation system for households in the Pacific Northwest, finding that traditional battery systems were more economically viable than PV/WT/FC/electrolyzer (EL) systems, emphasizing the importance of improving FC and EL efficiency. Maleki and Pourfayaz [32] performed a cost-benefit analysis of PV/WT/diesel/battery (BT)/FC systems using harmony search algorithms, comparing two hybrid power system scenarios. They found that, although traditional battery systems were more cost-effective, FC systems provided a more reliable energy supply. Regarding the economic optimization of FC, Yang *et al.* [33] developed an economic evaluation framework for SOFC systems based on a full lifecycle analysis method incorporating energy, material, environmental, and economic flows. They analyzed the CAPEX, financial net present value, internal rate of return, and payback period of a 2 kW natural gas SOFC system. Their study found that the system had good economic feasibility, and in sensitivity analyses of sales price, material costs, and manufacturing costs, the sales price had the greatest impact on net present value. Furthermore, the study examined the economic feasibility of natural gas SOFC systems under carbon price policies, discovering that the economic competitiveness of SOFCs decreased as carbon price increased, unless cleaner fuels, such as renewable gas or hydrogen, were used. Gibson *et al.* [34] proposed a method for comparing the economic feasibility of CHP systems based on FC, microturbines, and gas turbines (GT). The results indicated that under carbon pricing scenarios, FC-based systems exhibited the best economic potential in medium-sized cases. However, the payback period for FC systems was close to the system's lifetime, suggesting that CAPEX significantly impacts their economic feasibility. Sensitivity analysis further revealed that a 5% reduction in CAPEX could shorten the payback period by up to six months, indicating that reductions in CAPEX have a substantial effect on system economics.

The aforementioned studies mainly focus on the integration and economic analysis of FC systems, while the performance of FC systems under the influence of uncertainty factors has also received significant attention. Wang *et al.* [35] investigated an HFC-based IES and proposed a distributed robust optimization method to address the impact of WT and PV output fluctuations on system scheduling. The results indicated that an optimized scheduling approach could reduce the usage of energy supply devices, enhance the stability of energy storage devices, and lower OPEX. Similarly, Lu *et al.* [36] designed an economic operation strategy for IES in response to the uncertainty of PV generation output. By precisely constructing the thermal system operation model and the thermoelectric output control model of HFC, this strategy corrected the PV generation output prediction curve under uncertain solar radiation conditions. The findings showed that the economic operation strategy, which accounts for the uncertainty in PV generation, can effectively improve the energy utilization efficiency of the system, reduce OPEX, and enhance system reliability.

In summary, most current research primarily focuses on the technical performance of HFC and their applications in microgrids or the transportation sector, while there is a gap in studies regarding the economic variability of HFC under different load demand conditions in Industrial Park IES [31–34]. Furthermore, existing studies often lack systematic modelling and optimization analysis of the uncertainties associated with load demands and the output of wind and solar energy, resulting in insufficient quantification of the regulation capabilities of HFC within IES [36]. Most research emphasizes operational scheduling optimization of the system, but there is a lack of analysis on the impact of HFC on the system, and limited exploration of the stability role of HFC under random fluctuations in the system [35].

This study aims to develop an MILP model to minimize the total annual cost of the system, focusing on the economic feasibility and system integration strategies of SOFC in distributed IES. By considering the impact of various key parameters, the optimal configuration of the system in different application scenarios is explored. Given the uncertainties in the system, this paper further incorporates robust optimization methods to assess the adaptability of SOFC under various scenarios, providing the theoretical foundation and technical support for the promotion and application of SOFC in distributed IES.

The main contributions of this study are as follows:

(1) Based on a real-world case study, a multi-dimensional parametric sensitivity analysis framework is developed to

systematically reveal the impacts of carbon price policies, fuel prices, demand structures, and technological characteristics of equipment on the economic feasibility of FC.

(2) Within an electricity–hydrogen integrated energy system, the impacts of FC integration on system economics, carbon emissions, and renewable energy utilization are systematically evaluated, and their carbon mitigation potential and economic contributions are quantitatively assessed.

(3) Employing a robust optimization approach to account for uncertainties in load and renewable energy output, and assessing the role of FC in enhancing system operational stability.

2. Problem Statement

This study aims to introduce SOFC technology into the IES of industrial parks to enhance the utilization of renewable energy and system stability and meet the comprehensive demands of the park for electricity, heat, cooling, and hydrogen. Addressing the issues of traditional energy systems, which rely on fossil fuels, have high carbon emissions, and exhibit low energy efficiency, this study constructs a multi-energy complementary framework that includes WT, PV, alkaline electrolyzer (ALK), SOFC, and energy storage systems. By optimizing the system composition and configuration, the study seeks to improve both the economic performance and sustainability of the system.

The energy demand in industrial parks is complex and diverse, encompassing electricity, thermal energy, cooling energy, and hydrogen energy. Traditional energy supply methods mainly rely on fossil fuels such as natural gas. While they can meet the basic energy needs of the system, they are associated with low energy utilization efficiency, high carbon emissions, poor system flexibility, and excessive dependence on external energy sources, making it difficult to adapt to the increasingly diversified, efficient, and low-carbon energy demands of industrial parks. Therefore, constructing an IES that incorporates renewable energy to provide cleaner and more efficient energy solutions for the park is of significant research value.

To increase the utilization of renewable energy and reduce fossil fuel consumption, industrial parks can adopt a multi-energy complementary structure incorporating WT, PV, and energy storage systems. In this system, wind and solar energy are the primary renewable energy sources, with energy storage devices used to regulate the energy supply and demand balance. However, due to the intermittency and variability of wind and solar resources, the system may experience excess electricity when renewable energy output is high, and rely on fossil fuels to supplement energy when output is low or demand is high. This model limits the utilization of renewable energy, leading to wind and solar power curtailment when clean energy cannot be consumed in time, affecting the system's economic performance and its level of decarbonization. Additionally, while energy storage devices can alleviate renewable energy fluctuations to some extent, their regulation capacity is limited by storage capacity, charge-discharge efficiency, and operational cost.

To improve the utilization efficiency of renewable energy and enhance the system's regulation capability, this study proposes integrating SOFC, which uses hydrogen as its fuel, into the existing IES. By combining hydrogen storage (HST) and ALK technology to construct the EH-IES shown in Fig. 1, achieving the complementary conversion of electrical and hydrogen energy. When renewable energy output is surplus, the system converts electrical energy into hydrogen for storage *via* water electrolysis. During peak load periods or when renewable energy output is insufficient, the stored hydrogen is efficiently converted back into electricity using the SOFC, thereby enhancing the system's stability and energy utilization. Moreover, SOFC can not only be used for power generation but can also be integrated into CHP systems, improving overall energy utilization efficiency. This power-hydrogen coordination model not only alleviates the fluctuation issues of renewable energy but also optimizes the energy supply structure in industrial parks through multi-energy complementarity.

To evaluate the economic viability and system integration value of SOFC, this study constructs an optimization model intending to minimize the total annual cost of the system. The study compares and analyzes two systems: one with and one without the integration of SOFC, focusing on the impact of SOFC on system economics and CO_2 emissions. Given that the high initial capital cost of SOFC may affect their economic feasibility, a sensitivity analysis is conducted to examine the influence of key economic factors such as carbon price, energy demand, equipment efficiency, fuel prices, and HFC lifespan on the optimization results. Furthermore, to investigate the impact of wind and solar resource variability and load demand uncertainty on system economics and stability, this study employs robust optimization methods to analyze the effects of wind and solar output and load demands on system economics, as well as the role of HFC in enhancing system stability. The findings can provide a theoretical basis for the rational allocation of HFC in industrial parks and offer insights into the optimization of integrated energy systems in similar regions.

3. Optimization Problem Model

This study establishes a model with the total annual cost of the system as the objective function, considering various constraints. It is assumed that the system operates continuously throughout the year, with data such as the annual energy demand, energy prices, and equipment parameters used as input parameters for the model. The capacity of the equipment and the energy input to the equipment are taken as decision variables.

3.1. Objective function

The optimization objective of this study is to minimize the total annual cost C_{Tot} of the IES. The C_{Tot} consists of capital investment cost C_i, fuel cost C_{fuel}, and the cost of carbon emission C_{emission}. The mathematical formulation of the objective function is presented in Eq. (1), while the calculation method for investment cost is detailed in Eq. (2).

$$\min C_{\mathrm{Tot}} = C_i + C_{\mathrm{fuel}} + C_{\mathrm{emission}} \tag{1}$$

$$C_i = \sum_f B_f W_f \left(C_f^{\mathrm{O\&M}} + C_f^{\mathrm{INV}} \frac{i(i+1)^{n_f}}{(i+1)^{n_f}-1} \right), f \in F \tag{2}$$

The cost of natural gas fuel is related to the price and consumption of natural gas and is calculated as shown in Eqs. (3) and (4). The carbon emissions of the system also originate from natural gas, and the cost of carbon emission, which is related to the carbon price and the amount of carbon emissions, is calculated as shown in Eq. (5).

$$p_{t,\mathrm{gas}} = \frac{P_{t,\mathrm{GT}} + P_{t,\mathrm{DB}}}{\Phi H_{\mathrm{CH_4}}}, t \in NT \tag{3}$$

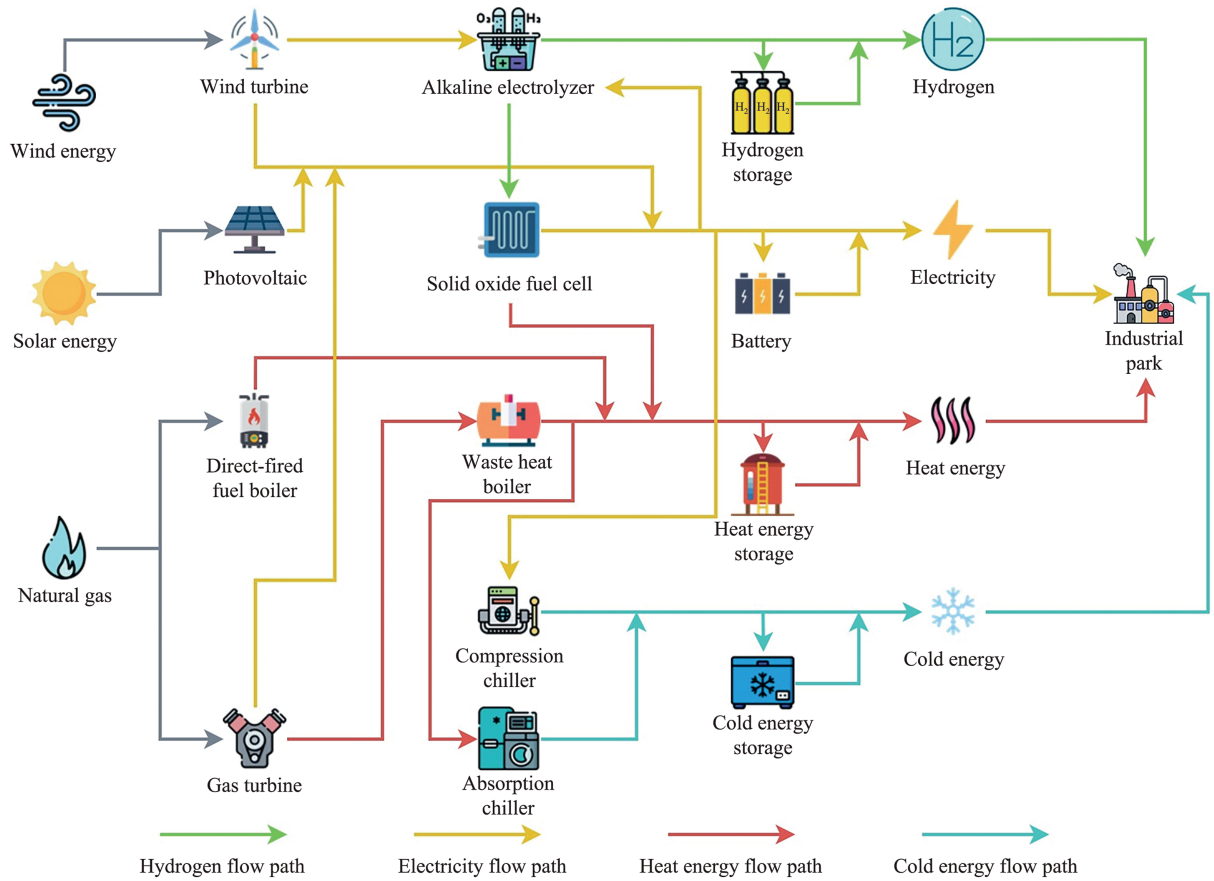


Fig. 1. Schematic diagram of the integrated energy system structure with hydrogen fuel cells.

$$C_{\text{fuel}} = \sum_{t\in T} P_{t,\text{gas}} CE_{\text{gas}}, t \in NT \tag{4}$$

$$C_{\text{emission}} = \sum_{t\in T} P_{t,\text{gas}} EF_{\text{gas}} CE_{\text{emission}}, t \in NT \tag{5}$$

3.2. Wind power generation model

$$P_t^{\text{WT}} = \eta^{\text{WT,System}} \sum_{j=1}^{n^{\text{WT}}} P_{t,j}^{\text{WT}}, t \in NT \tag{6}$$

$$P_{t,j}^{\text{WT}} = \begin{cases} 0, v_t < v^{\text{Cut-in}} \text{ or } v_t > v^{\text{Cut-out}} \\ \frac{1}{2}\eta^{\text{WT}} \rho^{\text{Air}} \pi \left(R^{\text{WT}}\right)^2 v_t^3, v^{\text{Cut-in}} < v_t < v^{\text{Rated}}, t \in NT \\ P^{\text{WT,Rated}}, v^{\text{Rated}} \le v_t \le v^{\text{Cut-out}} \end{cases} \tag{7}$$

$$v_t = \frac{\ln\left(\frac{H^{\text{WT}}}{z^0}\right)}{\ln\left(\frac{H^{\text{Obs}}}{z^0}\right)} v_t^{\text{Obs}}, t \in NT \tag{8}$$

The output power of a single WT at time t, $P_{t,j}^{\text{WT}}$, and the total output power of the WT group at time t, P_t^{WT}, are calculated using Eq. (6) [37]. Here, n^{WT} represents the number of WTs, while $\eta^{\text{WT,System}}$ and η^{WT} denote the efficiency of the wind power system and the efficiency of a single WT, respectively. $v^{\text{Cut-in}}$, $v^{\text{Cut-out}}$, v^{Rated}, ρ^{Air}, R^{WT}, and $P^{\text{WT,Rated}}$ are the cut-in wind speed, cut-out wind speed, rated wind speed, air density, blade radius, and rated power of a single WT, respectively. The wind speed at the hub height of WT, v_t, is derived from the wind speed at the measurement height, v_t^{Obs}, as shown in Eqs. (7) and (8), where H^{WT} and H^{obs} are the hub height and measurement height, respectively, and z^0 is the surface roughness at the location of the WT [38].

3.3. Photovoltaic power generation model

$$P_t^{\text{PV}} = P^{\text{PV,Rated}} \eta^{\text{PV,System}} \eta^{\text{PV,Derating}} \left(\frac{I_t^{\text{G}}}{I^{\text{G,STC}}}\right) \left[1 + \lambda\left(T_t^{\text{PV}} - T^{\text{PV,STC}}\right)\right], t \in NT \tag{9}$$

$$\eta^{\text{PV,Derating}} = \frac{1}{N^{\text{LC,PV}}} \sum_{k=1}^{N^{\text{LC,PV}}} \left[1 - \eta^{\text{PV,Derating,F}} \left(\eta^{\text{PV,Derating,A}}\right)^{k-1}\right] \tag{10}$$

The power generated by the PV system at time t, P_t^{PV} is calculated based on the incident solar radiation and ambient temperature, as shown in Eqs. (9) and (10) [39]. Here, $P^{\text{PV,Rated}}$ refers to the rated capacity of the PV system, by the PV system at time t, $P^{\text{PV,Rated}}$

is the rated capacity of the PV system, while $\eta^{PV,System}$ and $\eta^{PV,Derating}$ represent the operating efficiency of the PV system and the average derating factor of the PV modules, respectively. I_t^G and $I^{G,STC}$ are the incident solar irradiance at time t and under standard test conditions, respectively. λ is the power temperature coefficient, and T_t^{PV} and $T^{PV,STC}$ are the temperatures of the PV modules at time t and under standard test conditions, respectively. $\eta^{PV,Derating,F}$ and $\eta^{PV,Derating,A}$ are the derating factors for the first year and each year after the first year of the PV module's lifecycle, respectively. The derating factors are influenced by various elements, including the type correction factor of the PV modules, the tilt angle of the PV array, the azimuth angle correction factor, the availability of the PV power generation system, the utilization rate of sunlight, the efficiency of the inverter, grid connection losses, step-up transformer losses, surface contamination correction factor of the PV modules, and the conversion efficiency correction factor of the PV modules.

3.4. Constraints

3.4.1. Energy balance constraints

To ensure continuous and normal production and living needs within the industrial park, the model's constraints include energy balance, energy supply, and technical limitations. To guarantee smooth operations, the electricity generated by the distributed energy system minus the electricity consumed should be greater than or equal to the park's electricity demand. The compression chiller (COC) converts electrical energy into cooling energy, and this constraint is detailed in Eq. (11).

$$P_t^{WT} + P_t^{PV} + \eta_{GT,elec}P_{t,GT} - P_{t,COC} + \eta_{FC,elec}P_{t,FC} - P_{t,ALK} + N_{t,BT}^{dis} - N_{t,BT}^{ch} \geq D_t^{elec}, t \in NT \tag{11}$$

Heating equipment primarily consists of direct-fired fuel boilers (DB), waste heat boilers (WB), and SOFC. Absorption chillers (ABC) produce cooling by consuming heat. In this context, the thermal energy generated by the distributed energy system minus the heat used for cooling should be greater than or equal to the thermal energy demand of the industrial park. This constraint is outlined in Eq. (12).

$$\eta_{WB,heat}P_{t,WB} + \eta_{DB,heat}P_{t,DB} - P_{t,ABC} + \eta_{FC,heat}P_{t,FC} + N_{t,HS}^{dis} - N_{t,HS}^{ch} \geq D_t^{heat}, t \in NT \tag{12}$$

The cold energy generated by the distributed energy system should meet or exceed the cooling demand of the industrial park, as constrained by Eq. (13). The park is equipped with both COC and ABC for cooling purposes.

$$COP_{COC}P_{t,COC} + COP_{ABC}P_{t,ABC} + N_{t,CS}^{dis} - N_{t,CS}^{ch} \geq D_t^{cool}, t \in NT \tag{13}$$

If there is a demand for hydrogen in the industrial park, the system should ultimately produce an amount of hydrogen that is greater than or equal to the hydrogen energy demand of the park, as constrained by Eq. (14).

$$P_{t,ALK}^{hydrogen} - P_{t,FC}^{hydrogen} + N_{t,HST}^{out} - N_{t,HST}^{in} \geq D_t^{hydrogen}, t \in NT \tag{14}$$

The operation of energy storage devices is related to their charging and discharging rates as well as energy losses, hence, the constraints on the operational status of energy storage equipment are presented in Eqs. (15) and (16). Furthermore, to ensure that the energy storage devices operate more realistically and maintain stable operation when activated, constraints on the amount of energy stored when the devices are turned on are imposed, as shown in Eq. (17).

$$SP_{t,f} = \left(1 - \eta_f^{loss}\right)SP_{t-1,f} + \eta_f^{ch}N_{t,f}^{ch} - \frac{N_{t,f}^{dis}}{\eta_f^{dis}}, f \in F, t \in NT \tag{15}$$

$$SP_{t,f} = \eta_f^{ch}N_{t,f}^{ch} - \frac{N_{t,f}^{dis}}{\eta_f^{dis}}, f \in F, t = 1 \tag{16}$$

$$SP_{1,f} = SP_{NT,f} = \frac{W_f}{2} \tag{17}$$

For the storage and release of hydrogen, the operational constraints of the HST are detailed in Eqs. (18) and (19).

$$SP_{t,HST}^{hydrogen} = \left(1 - \eta_{HST}^{loss}\right)SP_{t-1,HST}^{hydrogen} + \eta_{HST}^{in}N_{t,HST}^{in} - \frac{N_{t,HST}^{out}}{\eta_{HST}^{out}}, t \in NT \tag{18}$$

$$SP_{t,HST}^{hydrogen} = \eta_{HST}^{in}N_{t,HST}^{in} - \frac{N_{t,HST}^{out}}{\eta_{HST}^{out}}, t = 1 \tag{19}$$

3.4.2. Technical constraints

The rated capacity of any equipment must not exceed its maximum capacity, as constrained in Eq. (20). During the operation of each functional device, the energy input must not surpass the device's rated capacity, which is governed by Eq. (21). In the case of energy storage devices, the energy stored at any given moment must not exceed the device's rated capacity, a constraint outlined in Eq. (22).

$$\left(B_f - 1\right)W_{max} \leq W_f \leq B_f W_{max}, f \in F \tag{20}$$

$$P_{t,f} \leq W_f, f \in F, t \in NT \tag{21}$$

$$SP_{t,f} \leq W_f, f \in F, t \in NT \tag{22}$$

The energy input to the WB should be equal to the heat output of the GT, with this constraint detailed in Eq. (23). The energy input to the ABC should not exceed the heat output of the WB, a constraint specified in Eq. (24).

$$P_{t,WB} = \eta_{GT,heat}P_{t,GT}, t \in NT \tag{23}$$

$$P_{t,ABC} \leq \eta_{WB,heat}P_{t,WB}, t \in NT \tag{24}$$

The relationship between the output power of the SOFC and the input power of hydrogen is shown in Eq. (25). The relationship between the hydrogen production efficiency of the ALK and the input power of the ALK is depicted in Eq. (26).

$$P_{t,FC} = H_{H_2}P_{t,FC}^{hydrogen}, t \in NT \tag{25}$$

$$P_{t,ALK}^{hydrogen} = \frac{\eta_{ALK,hydrogen}P_{t,ALK}}{H_{H_2}}, t \in NT \tag{26}$$

3.5. Consider uncertainty optimization

In the presence of uncertainties related to wind and solar power generation, as well as demands for electricity, thermal, cold, and hydrogen, it is essential to ensure the system's normal operation by employing robust optimization methods for constraint handling. Following the robust optimization approach proposed by Bertsimas and Sim [40], uncertain variables are assigned to uncertainty sets, and the system constraints are adjusted by introducing control parameters that regulate the model's conservativeness and uncertainty disturbance coefficients. This ensures that the system can meet demands at various levels of uncertainty. Considering the uncertainties in wind and solar power generation, as well as electricity, thermal, cold, and hydrogen demands, the corresponding constraints are adjusted as shown in Eqs. (27)–(35).

$$Z_t + P_{t,1} \geq \widehat{a}_t, t \in NT \tag{27}$$

$$Z_t \geq 0, t \in NT \tag{28}$$

$$P_{t,1} \geq 0, t \in NT \tag{29}$$

$$P_t^{\mathrm{WT}} + P_t^{\mathrm{PV}} + \eta_{\mathrm{GT,elec}} P_{t,\mathrm{GT}} - P_{t,\mathrm{COC}} + \eta_{\mathrm{FC,elec}} P_{t,\mathrm{FC}} - P_{t,\mathrm{ALK}} + N_{t,\mathrm{BT}}^{\mathrm{dis}} - N_{t,\mathrm{BT}}^{\mathrm{ch}} \geq \overline{D}_t^{\mathrm{elec}} + \left(Z_t \Gamma + \sum P_{t,1}\right), t \in NT \tag{30}$$

$$\eta_{\mathrm{WB,heat}} P_{t,\mathrm{WB}} + \eta_{\mathrm{DB,heat}} P_{t,\mathrm{DB}} - P_{t,\mathrm{ABC}} + \eta_{\mathrm{FC,heat}} P_{t,\mathrm{FC}} + N_{t,\mathrm{HS}}^{\mathrm{dis}} - N_{t,\mathrm{HS}}^{\mathrm{ch}} \geq \overline{D}_t^{\mathrm{heat}} + \left(Z_t \Gamma + \sum P_{t,1}\right), t \in NT \tag{31}$$

$$\mathrm{COP}_{\mathrm{COC}} P_{t,\mathrm{COC}} + \mathrm{COP}_{\mathrm{ABC}} P_{t,\mathrm{ABC}} + N_{t,\mathrm{CS}}^{\mathrm{dis}} - N_{t,\mathrm{CS}}^{\mathrm{ch}} \geq \overline{D}_t^{\mathrm{cool}} + \left(Z_t \Gamma + \sum P_{t,1}\right), t \in NT \tag{32}$$

$$P_{t,\mathrm{ALK}}^{\mathrm{hydrogen}} - P_{t,\mathrm{FC}}^{\mathrm{hydrogen}} + N_{t,\mathrm{HST}}^{\mathrm{out}} - N_{t,\mathrm{HST}}^{\mathrm{in}} \geq \overline{D}_t^{\mathrm{hydrogen}} + \left(Z_t \Gamma + \sum P_{t,1}\right), t \in NT \tag{33}$$

$$\overline{P}_t^{\mathrm{WT}} - \left(Z_t \Gamma + \sum P_{t,1}\right) + P_t^{\mathrm{PV}} + \eta_{\mathrm{GT,elec}} P_{t,\mathrm{GT}} - P_{t,\mathrm{COC}} + \eta_{\mathrm{FC,elec}} P_{t,\mathrm{FC}} - P_{t,\mathrm{ALK}} + N_{t,\mathrm{BT}}^{\mathrm{dis}} - N_{t,\mathrm{BT}}^{\mathrm{ch}} \geq D_t^{\mathrm{elec}}, t \in NT \tag{34}$$

$$P_t^{\mathrm{WT}} + \overline{P}_t^{\mathrm{PV}} - \left(Z_t \Gamma + \sum P_{t,1}\right) + \eta_{\mathrm{GT,elec}} P_{t,\mathrm{GT}} - P_{t,\mathrm{COC}} + \eta_{\mathrm{FC,elec}} P_{t,\mathrm{FC}} - P_{t,\mathrm{ALK}} + N_{t,\mathrm{BT}}^{\mathrm{dis}} - N_{t,\mathrm{BT}}^{\mathrm{ch}} \geq D_t^{\mathrm{elec}}, t \in NT \tag{35}$$

3.6. Solution method

The proposed optimization model is implemented in MATLAB and solved using the commercial solver GUROBI. The model aims to determine the minimum total annual cost of the industrial park's energy system while identifying the optimal operational strategy for system components. Additionally, the study evaluates the economic benefits of integrating SOFC and accounts for uncertainties within the system parameters.

4. Case Study

A case study is conducted for an industrial park in Baotou, China, to analyze the optimal configuration of its IES. The park has access to wind and solar energy resources and demands for electricity, heat, cooling, and hydrogen. To enhance energy efficiency and reduce dependence on external energy sources, the study proposes an energy system incorporating WT, PV, SOFC, and energy storage. Furthermore, employing robust optimization methods to investigate the impact of wind and solar energy output fluctuations and load demand uncertainties on system economics.

4.1. Wind and solar resources

The wind and solar resource data used in this study were obtained from NASA's Power Data Access Viewer platform. The wind speed and solar irradiance distributions for the year are illustrated in Fig. 2. The minimum, average, and maximum wind speeds were recorded at 0.05 m·s^{-1}, 5.81 m·s^{-1}, and 22.1 m·s^{-1}, respectively.

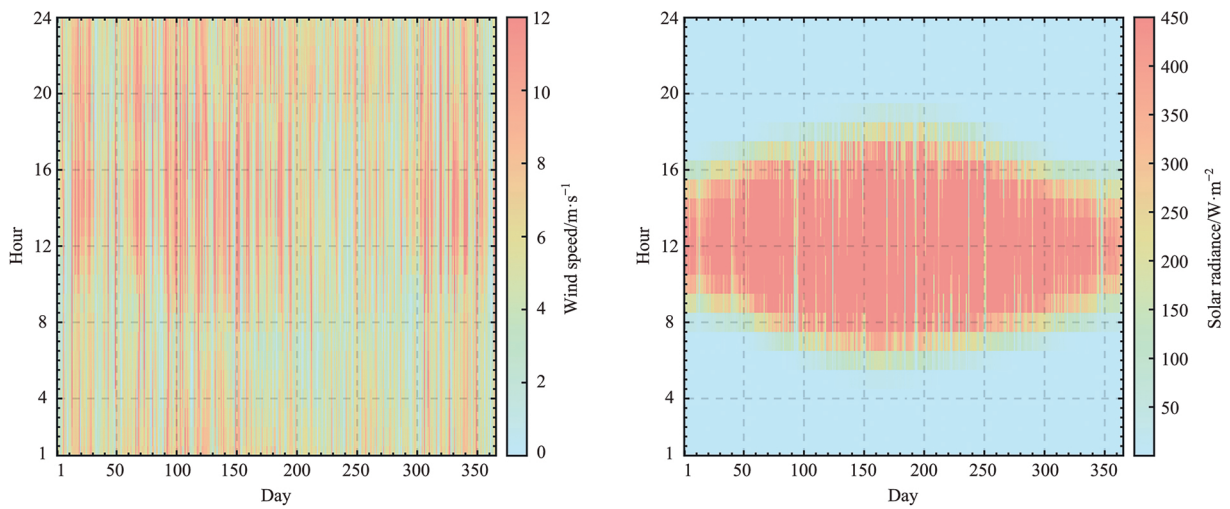


Fig. 2. Measured wind speed and solar irradiance.

The minimum, average, and maximum solar irradiances were 0.00 $W \cdot m^{-2}$, 204.62 $W \cdot m^{-2}$, and 1025.47 $W \cdot m^{-2}$, respectively.

This region benefits from abundant wind and solar resources, providing a strong foundation for advancing PV and wind power industries while fostering the development of hydrogen energy and energy storage as strategic emerging industries. Additionally, Baotou City is actively exploring an integrated "wind-solar-hydrogen-storage" coupling technology, leveraging renewable energy sources for hydrogen production to support the growth of the hydrogen energy sector. These practical outcomes not only provide a realistic basis for this study but also demonstrate the broad prospects for enhancing energy efficiency and reducing carbon emissions through the optimization of integrated energy systems, thereby promoting the green and low-carbon development of industrial parks.

4.2. Equipment parameters

To meet the energy demands of the industrial park, the system includes GT, WT, PV, DB, WB, COC, ABC, ALK, SOFC, and energy storage systems. The maximum capacities and cost parameters of various system components are summarized in Table 1, while the technical specifications of these components are detailed in Table 2. The relevant parameters of the WT are shown in Table 3.

Table 2
Equipment technical parameters [41,42,44].

Equipment	$\eta_{f,\mathrm{elec}}$	$\eta_{f,\mathrm{heat}}$	$\eta_{\mathrm{ALK,hydrogen}}$	COP	η_f^{loss}	η_f^{ch}	η_f^{dis}
GT	0.35	0.55	—	—	—	—	—
WT	0.69	—	—	—	—	—	—
PV	0.90	—	—	—	—	—	—
DB	—	0.95	—	—	—	—	—
WB	—	0.65	—	—	—	—	—
COC	—	—	—	4.5	—	—	—
ABC	—	—	—	1.37	—	—	—
BT	—	—	—	—	0.01	0.90	0.90
HS	—	—	—	—	0.01	0.90	0.90
CS	—	—	—	—	0.01	0.90	0.90
HST	—	—	—	—	0.01	0.99	0.99
ALK	—	—	0.845	—	—	—	—
HFC	0.49	0.31	—	—	—	—	—

Table 3
Individual wind turbine model parameters [41,42,44].

Parameter	Value
H^{WT}/m	110
H^{Obs}/m	10
$P^{\mathrm{WT,Rated}}$/kW	6250
R^{WT}/m	96.5
$v^{\mathrm{Cut\text{-}in}}/m \cdot s^{-1}$	3
$v^{\mathrm{Cut\text{-}out}}/m \cdot s^{-1}$	20
$v^{\mathrm{Rated}}/m \cdot s^{-1}$	10.2

5. Result and Analysis

5.1. Economic benefit evaluation

As shown in Fig. 3, the optimization results indicate that the installed capacity of the SOFC is zero, suggesting that under the current system conditions, SOFCs are not included in the optimal configuration. The primary reason lies in the high capital and operational costs of SOFC. Compared to GT, DB, and WB, the cost per unit power of SOFC is significantly higher than those technologies. Furthermore, the economic feasibility of SOFC is closely related to hydrogen production costs. In the system, hydrogen production *via* water electrolysis is also affected by electricity prices and electrolysis efficiency, resulting in a relatively poor economic performance of the electricity-hydrogen energy complementarity system. Consequently, under the objective of minimizing costs, the optimization results favour selecting lower-cost and higher-efficiency equipment, such as GT and direct energy storage, rather than SOFC as a primary energy supply technology.

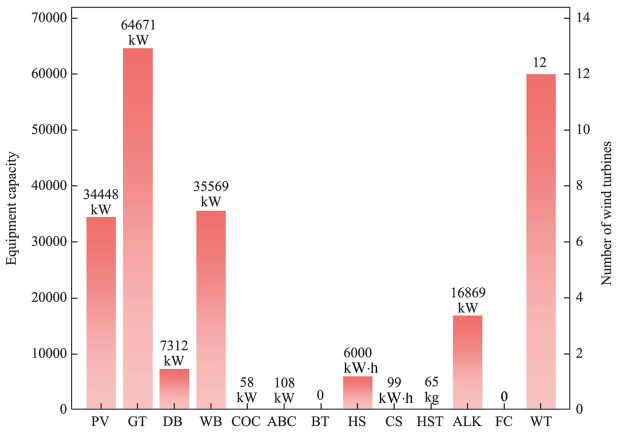


Fig. 3. Energy system equipment configuration scheme.

Table 1
Equipment cost parameters [41–43].

Equipment	Maximum capacity	C_f^{INV}	$C_f^{\mathrm{O\&M}}$	Lifetime/a	Depreciation rate
GT	80000 kW	2150 CNY·kW^{-1}	21.5 CNY·kW^{-1}·a^{-1}	25	0.08
WT	20 unit	3800 CNY·kW^{-1}	38 CNY·kW^{-1}·a^{-1}	20	0.05
PV	80000 kW	3969 CNY·kW^{-1}	39.69 CNY·kW^{-1}·a^{-1}	20	0.05
DB	80000 kW	1490 CNY·kW^{-1}	14.9 CNY·kW^{-1}·a^{-1}	20	0.08
WB	80000 kW	1560 CNY·kW^{-1}	15.6 CNY·kW^{-1}·a^{-1}	20	0.08
COC	80000 kW	1236 CNY·kW^{-1}	12.36 CNY·kW^{-1}·a^{-1}	25	0.08
ABC	80000 kW	1893 CNY·kW^{-1}	18.93 CNY·kW^{-1}·a^{-1}	25	0.08
BT	6000 kW·h	1785 CNY·(kW·h)$^{-1}$	17.85 CNY·(kW·h)$^{-1}$·a^{-1}	20	0.08
HS	6000 kW·h	100 CNY·(kW·h)$^{-1}$	1 CNY·(kW·h)$^{-1}$·a^{-1}	20	0.08
CS	6000 kW·h	200 CNY·(kW·h)$^{-1}$	2 CNY·(kW·h)$^{-1}$·a^{-1}	20	0.08
HST	6000 kg	15.31 CNY·kg^{-1}	0.1531 CNY·kg^{-1}·a^{-1}	20	0.08
ALK	80000 kW	779 CNY·kW^{-1}	7.79 CNY·kW^{-1}·a^{-1}	20	0.08
HFC	80000 kW	2994 CNY·kW^{-1}	29.94 CNY·kW^{-1}·a^{-1}	7	0.15

Note: CS, cold energy storage; EL,electrolytic cell; GB, gas turbine; HS, thermal energy storage.

5.2. Sensitivity analysis

Since SOFCs were not included in the optimal configuration primarily due to high capital costs and operational costs, it is essential to further analyze their economic sensitivity to key economic factors. Energy prices, cost of facility, carbon price policies, and technological advancements may significantly influence the system optimization results and alter the economic feasibility of SOFC. Therefore, this section explores the minimum feasible cost of SOFC under different conditions through sensitivity analysis.

5.2.1. Sensitivity analysis of system energy demand

The impact of variations in electricity, thermal, cold, and hydrogen demands on system optimization results is examined, as shown in Fig. 4. The results indicate that changes in energy demand affect the minimum feasible cost of SOFC in the system. An increase in electricity and hydrogen demand leads to an increase in the minimum feasible cost of SOFC, suggesting a positive impact on their economic feasibility. Conversely, an increase in heat and cooling demand reduces the minimum feasible cost of SOFC, indicating a negative impact. The increase in electricity demand is most beneficial to SOFC economics, whereas the increase in heat demand is the least favourable. This suggests that within the system, SOFCs have a relative advantage in electricity generation costs but a disadvantage in heat production costs. Additionally, the cooling energy of the system is primarily derived from the conversion of electrical and thermal energy. An increase in the system's hydrogen demand can indirectly reduce hydrogen production costs, thereby lowering the fuel cost of SOFC.

5.2.2. Sensitivity analysis of equipment efficiency

The impact of changes in the efficiency of SOFC, ALK, GT, and DB on the minimum feasible price of SOFC is examined, as shown in Fig. 4. The results indicate that different equipment efficiencies have varying degrees of impact on the minimum feasible price of SOFC. Notably, an improvement in SOFC efficiency significantly increases the minimum feasible price of SOFC, whereas improvements in GT and DB efficiencies reduce the minimum feasible price. This suggests that under current cost conditions, enhancing SOFC efficiency helps lower the economic threshold for SOFC adoption in the system. Additionally, changes in ALK efficiency have a relatively minor impact on the minimum feasible price of SOFC, likely because improved ALK efficiency reduces electricity consumption, thereby limiting the role of SOFC.

5.2.3. Sensitivity analysis of carbon price

Carbon price vary by country, typically ranging from 7 CNY·(t CO_2)$^{-1}$ to 1010 CNY·(t CO_2)$^{-1}$ [45]. As shown in Fig. 5, the sensitivity analysis examines the impact of carbon price levels ranging from 7 to 1007 CNY·(t CO_2)$^{-1}$ on system optimization results. The results reveal that as the carbon price increases, the minimum feasible cost of SOFC exhibits a linear growth trend, rising from 2574.84 CNY·kW^{-1} to 5389.2 CNY·kW^{-1}. This is because higher carbon price increase the operational cost of fossil fuel-based equipment, making low-carbon or zero-carbon technologies more economically competitive. However, due to the still-high initial capital cost and operational cost of SOFC, they only become part of the optimal configuration when the carbon price level exceeds 187 CNY·(t CO_2)$^{-1}$.

5.2.4. Sensitivity analysis of natural gas prices

The impact of natural gas price variations on the minimum feasible price of SOFC is explored, as shown in Fig. 5. The results indicate that as natural gas prices increase, the minimum feasible price of SOFC exhibits a nonlinear growth trend. The rising natural gas prices increase the fuel cost of GT and DB, making SOFC more economically competitive. As a result, the system becomes more inclined to adopt SOFC. Under current system conditions, when the natural gas price exceeds 5.2 CNY·m^{-3}, the optimal configuration employs SOFC.

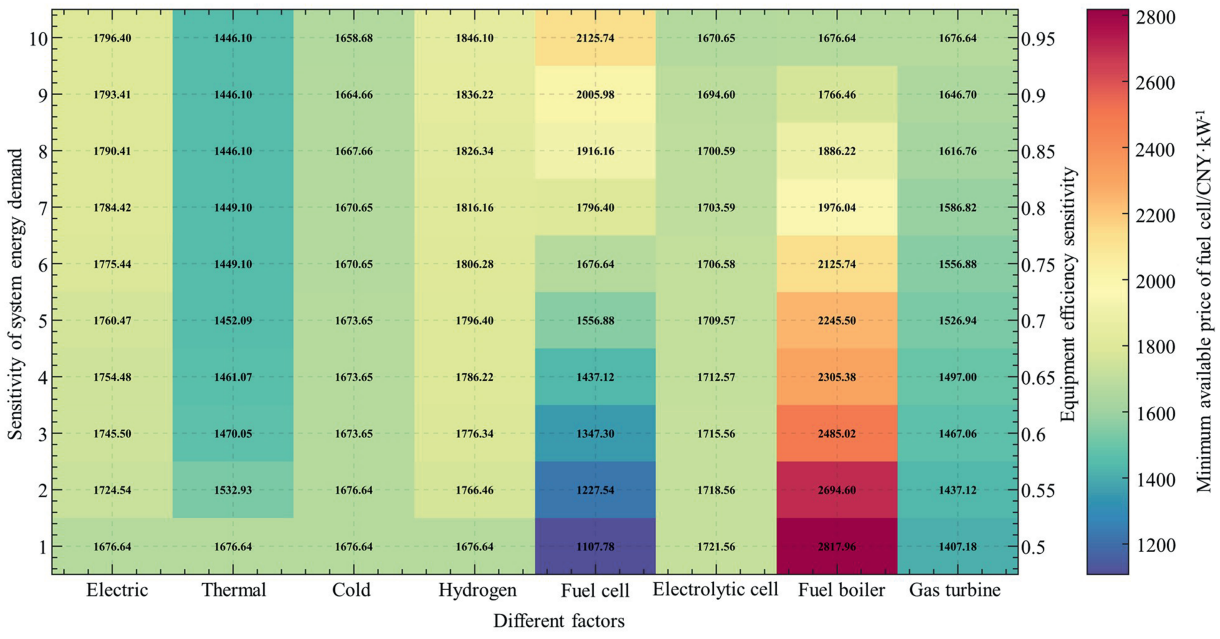


Fig. 4. Sensitivity analysis of energy demand and equipment efficiency.

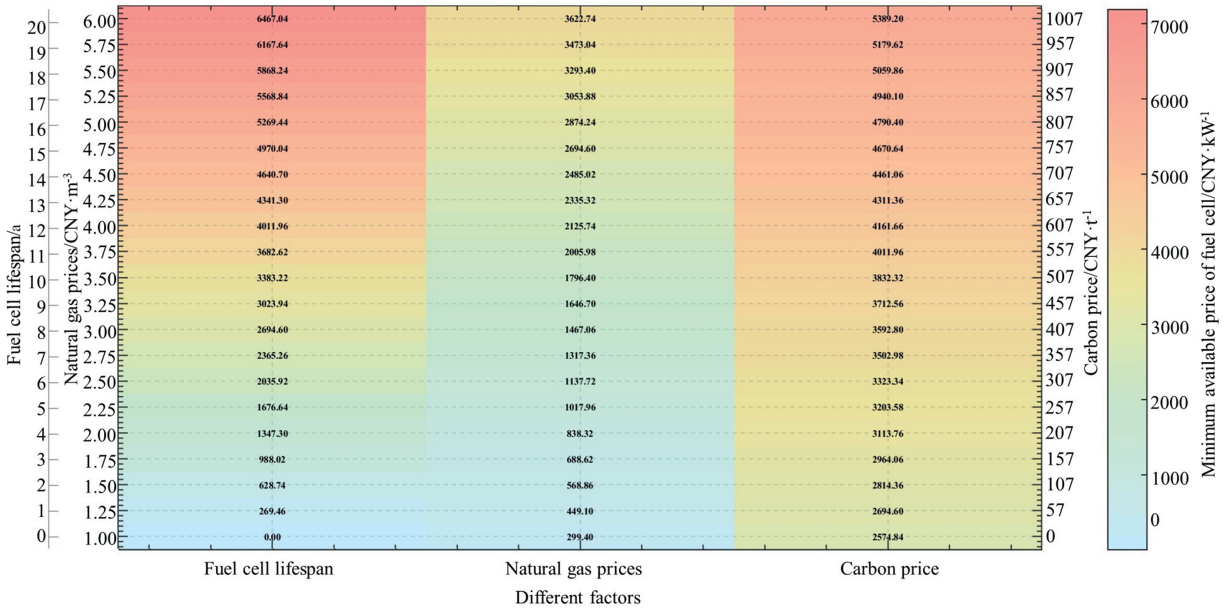


Fig. 5. Sensitivity analysis of fuel cell lifetime, natural gas prices, and carbon price.

5.2.5. Sensitivity analysis of fuel cell lifetime

The impact of SOFC lifetime on its minimum feasible price is examined, as shown in Fig. 5. The results indicate a linear positive correlation between SOFC lifetime and its minimum feasible price. As the lifetime extends from 1 year to 20 years, the minimum feasible price of SOFC increases linearly from 269.46 CNY·kW^{-1} to 6467.04 CNY·kW^{-1}. This demonstrates that the economic feasibility of SOFCs is highly dependent on their lifespan. Currently, most SOFCs have a lifespan of 5–10 years, and shorter lifespans limit their application in the system. Extending the lifespan could significantly improve their economic competitiveness.

5.3. Optimized system configuration

Given the potential economic benefits of SOFC under high carbon price environments, this study incorporates a carbon price mechanism into the existing energy system, setting the carbon price at 441.19 CNY·(t CO_2)$^{-1}$, and further analyzes the impact of SOFC integration on system economics and equipment configuration. As shown in Table 4, integrating SOFC reduces the system's total annual cost from 15.968 × 10^7 CNY to 15.936 × 10^7 CNY, a decrease of approximately 0.2%. Notably, the cost of carbon emission is significantly reduced from 2.292 × 10^{7}CNY to 2.114 × 10^7 CNY, a reduction of 7.8%, indicating that the low-carbon advantages of SOFC are realized in a high carbon price environment. However, the cost of the facility increased from 7.065 × 10^7 CNY to 7.723 × 10^7 CNY, an increase of approximately 9.3%, this indicates that the high capital cost of SOFC still has a certain impact on the system's economic viability.

Fig. 6 illustrates the structure of the optimized system. Due to the high capital cost of BT, the optimized system does not include BT. In the system incorporating SOFC, SOFC serves as the core component for the complementary conversion of electrical and hydrogen energy. Through the electricity-hydrogen energy conversion mechanism of SOFC, surplus renewable energy is converted into hydrogen for storage, which can be efficiently converted back into electricity during peak demand periods, thereby achieving flexible energy regulation.

As illustrated in Fig. 7, the integration of SOFC leads to changes in the configuration of conventional power generation equipment. The installed capacities of WT and PV increase, indicating that SOFC deployment enhances the utilization of renewable energy sources. Furthermore, the inclusion of SOFC replaces certain high-carbon-emission generation technologies, such as DB, whose installed capacity significantly decreases. Additionally, energy storage configurations adjust to accommodate the new energy supply-demand dynamics.

With SOFC integration, the system's annual renewable energy generation increases from 3.05 × 10^8 kW·h to 3.22 × 10^8 kW·h, reflecting a 5.72% expansion. Furthermore, after integrating SOFC into the system, the curtailment rate of electricity decreased by 7.1%, enhancing the utilization rate of renewable resources. This optimized configuration not only reduces the total annual cost but

Table 4
Results of economic and environmental benefits.

Result	Scenario	
	The system without SOFC integrated	The system with SOFC integrated
Total annual cost/10^{7}CNY	15.968	15.936
Cost of facility/10^{7}CNY	7.065	7.723
Cost of energy/10^{7}CNY	6.611	6.099
Cost of carbon emission/10^{7}CNY	2.292	2.114

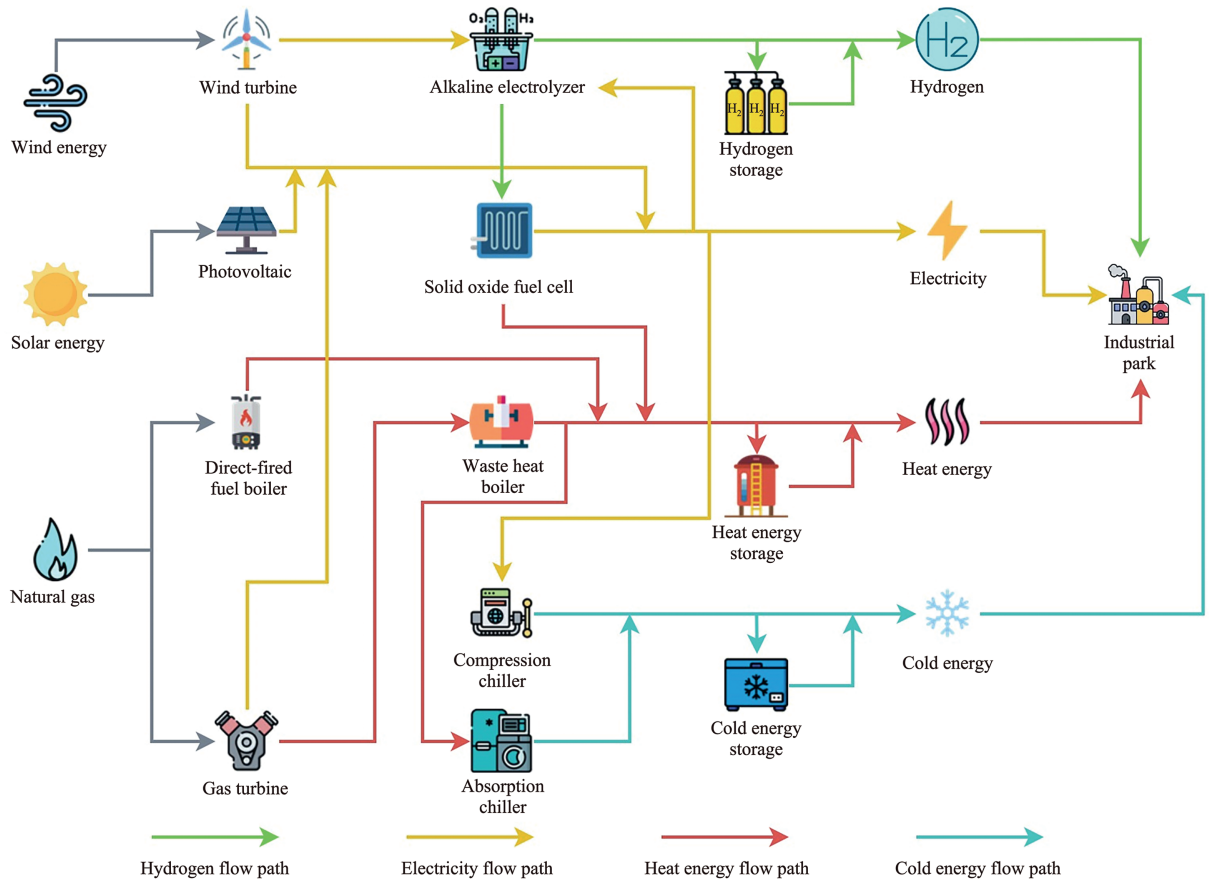


Fig. 6. Schematic diagram of the optimized integrated energy system.

also lowers carbon emissions while effectively increasing the share of renewable energy in the energy mix.

Figs. 8 and 9 depict the hourly energy dispatch of the electricity-hydrogen module in systems without and with SOFC integration, respectively. In the system without SOFC, hydrogen production through electrolysis primarily relies on intermittent renewable energy generation. However, due to the lack of an effective electrical-hydrogen energy complementary mechanism within the system, some renewable energy resources are abandoned due to mismatched demand, resulting in significant fluctuations in power output, and the potential of wind and solar resources remains underutilized.

In the system with integrated SOFCs, SOFCs function as the core component of the electricity-hydrogen conversion process. During periods of surplus renewable energy, electricity is converted into hydrogen for storage, which can later be reconverted into electricity during peak demand periods. This bidirectional energy exchange mitigates fluctuations in power output. Compared to the system without SOFC, the system with SOFC integration exhibits smoother power output, demonstrating that SOFCs play a crucial role in peak shaving and valley filling, ultimately enhancing the utilization rate of renewable energy.

Despite the 7.8% reduction in the cost of carbon emission following SOFC integration, the total annual cost decreased by only 0.2%. This finding highlights that under current economic conditions, SOFC remains constrained by high capital costs. Nonetheless, at a carbon price of 441.19 CNY·(t CO_2)$^{-1}$, SOFC integration reduces system CO_2 emissions from 51950 t to 47916 t, achieving a total reduction of approximately 4035 t CO_2, which demonstrates its clear carbon-mitigation benefits. Moreover, SOFC integration enhances renewable energy utilization, further supporting the system's low-carbon transition.

5.4. System uncertainty analysis

In practical operations, energy systems are subject to multiple uncertainties, including fluctuations in electricity, heat, cooling, and hydrogen demand, as well as WT and PV power generation variability. These uncertainty factors significantly impact system economics, stability, and optimization strategies. To address these challenges, this study employs a robust optimization model to comprehensively analyze system performance under various uncertainty conditions and assess the role of SOFC in maintaining system stability. The model considers six primary uncertainty factors: electricity demand, heat demand, cooling demand, hydrogen demand, and fluctuations in WT and PV power generation. By comparing systems with and without SOFC integration, this study evaluates the impact of these uncertainties on the total annual cost and explores how SOFC contributes to system stability under different uncertainty factors.

The control parameter Γ in the robust optimization model has a step size of 0.1, ranging from 0 to 1, while the perturbation coefficient ϕ of uncertain parameters has a step size of 0.05, ranging from 0 to 0.5. When $\Gamma = 0$, the model is equivalent to a

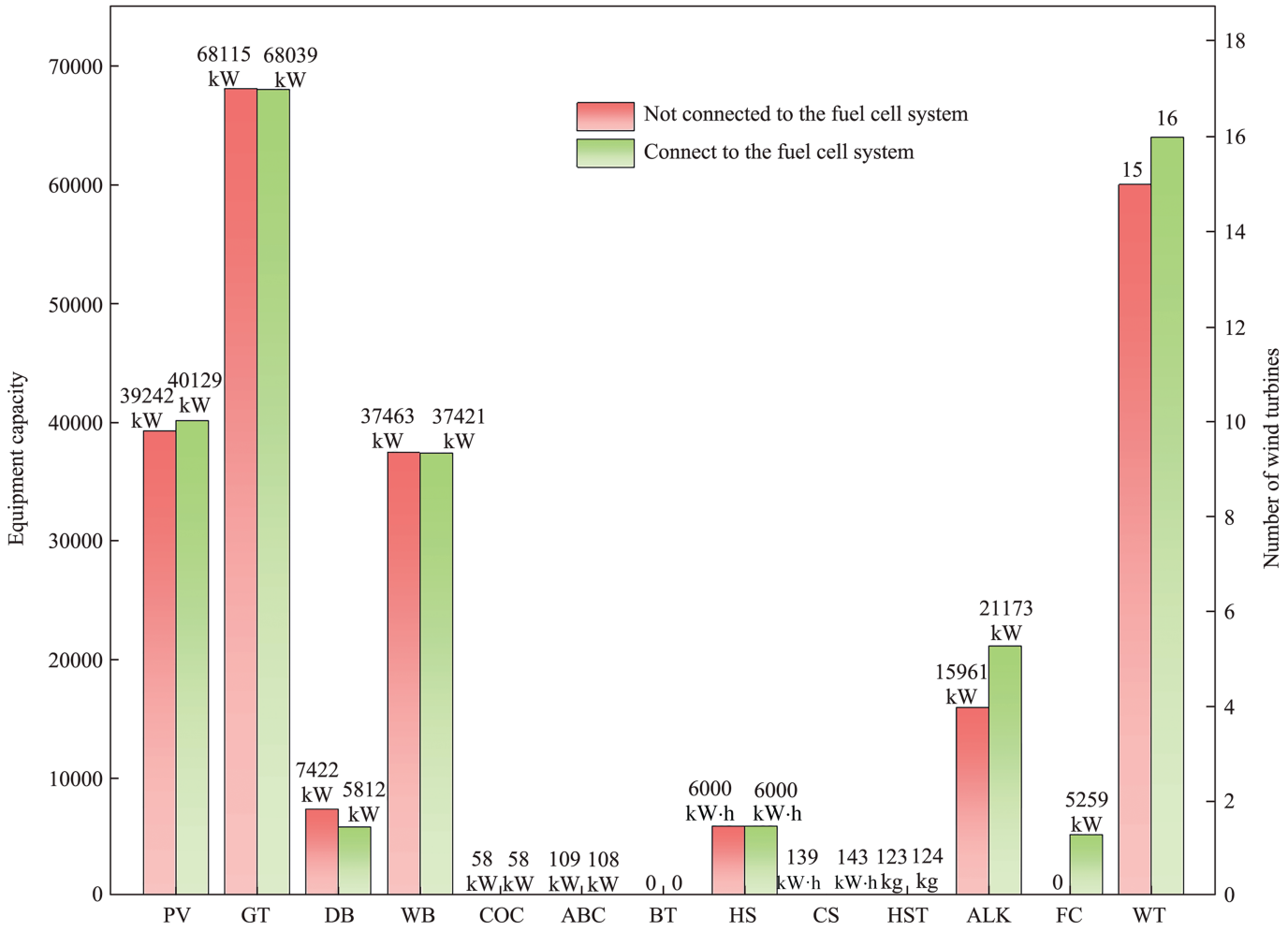


Fig. 7. System equipment configuration scheme.

deterministic model, representing the least conservative approach with the lowest total annual cost. As Γ increases, the model's robustness and resistance to uncertainty improve, but this comes at the expense of a higher total annual cost. The perturbation coefficient ϕ reflects the deviation of uncertain parameters from their nominal values, quantifying the intensity of uncertainty.

Fig. 10(a),(c),(e),(g),(i),(k) and (b),(d),(f),(h),(j),(l) quantify the sensitivity of total annual cost to stochastic fluctuations in electricity, heating, cooling and hydrogen demands as well as in wind/solar outputs, before and after the integration of the SOFC. A comparative inspection of these figures reveals the following. Under different uncertainty scenarios, the role of SOFC shows significant differences. At $\phi = 0.5$ and $\Gamma = 1$, under scenarios of electricity demand uncertainty (as shown in Fig. 10(a) and (b)), the total annual cost of the system with SOFC integrated increased by 17.79%, compared to an increase of 17.83% for the system without SOFC. The inclusion of SOFC reduces the system's sensitivity to electricity demand fluctuations, demonstrating better cost efficiency and stability. However, under scenarios of thermal energy demand uncertainty (as shown in Fig. 10(c) and (d)), the total annual cost increased by 8.36% with the integration of SOFC, surpassing the 8.25% increase observed in systems without SOFC. This indicates that the introduction of SOFC has not effectively mitigated the impact of uncertainty in thermal energy demand but instead added complexity and cost to the system. Similarly, in scenarios of cold energy demand uncertainty (as shown in Fig. 10(e) and (f)), the total annual cost increased by 0.0151% with SOFC, compared to a 0.0146% increase in systems without SOFC. This result confirms the poor adaptability of SOFC to uncertainty in cooling energy demand.

Under scenarios of uncertainty in hydrogen demand (as shown in Fig. 10(g) and (h)), the total annual cost increased by 24.46% with the integration of SOFC, which is lower than the 24.54% increase in systems without SOFC, indicating that SOFC can enhance system stability under conditions of uncertainty in hydrogen demand. In scenarios of wind power generation uncertainty (as shown in Fig. 10(i) and (j)), the total annual cost increased by 15.58% with SOFC, higher than the 15.35% increase in systems without SOFC. In scenarios of PV power generation uncertainty (as shown in Fig. 10(k) and (l)), the total annual cost increased by 6.96% with SOFC, higher than the 6.81% increase in systems without SOFC. Therefore, under scenarios of uncertainty in wind and solar power generation, SOFC did not enhance the stability of the system.

Overall, the effectiveness of SOFC is highly dependent on the type of uncertainty factors present. Under electricity and hydrogen demand uncertainties, SOFC significantly alleviates system cost increases, enhancing both economic performance

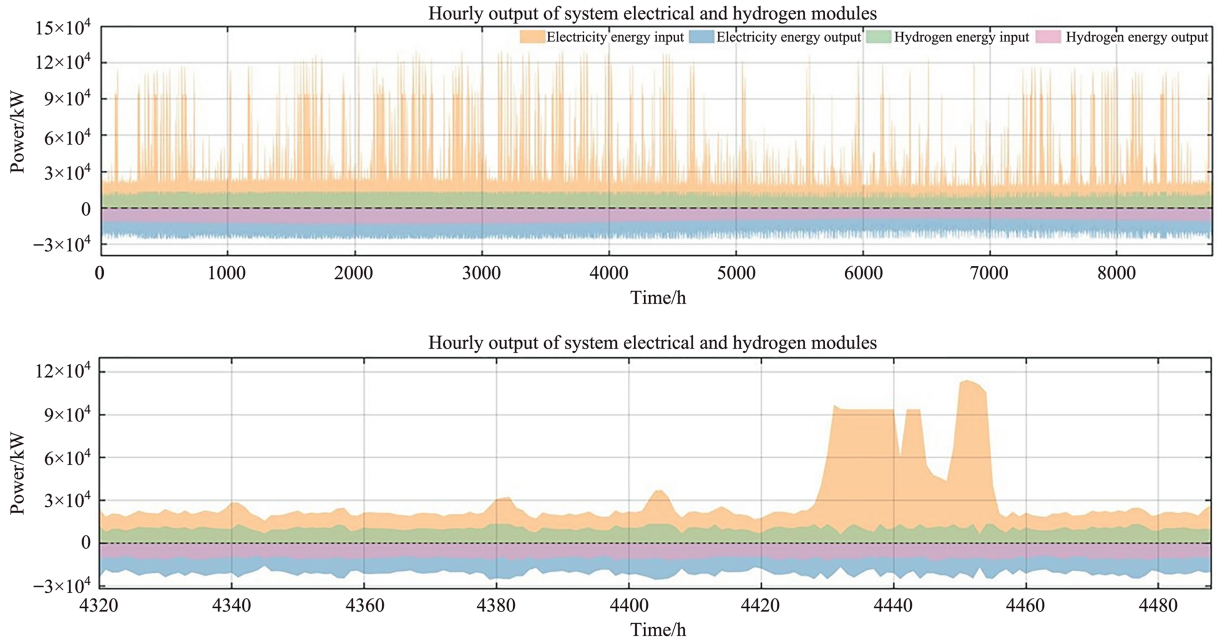


Fig. 8. Hourly energy output of the electricity-hydrogen module in a system without fuel cells integrated.

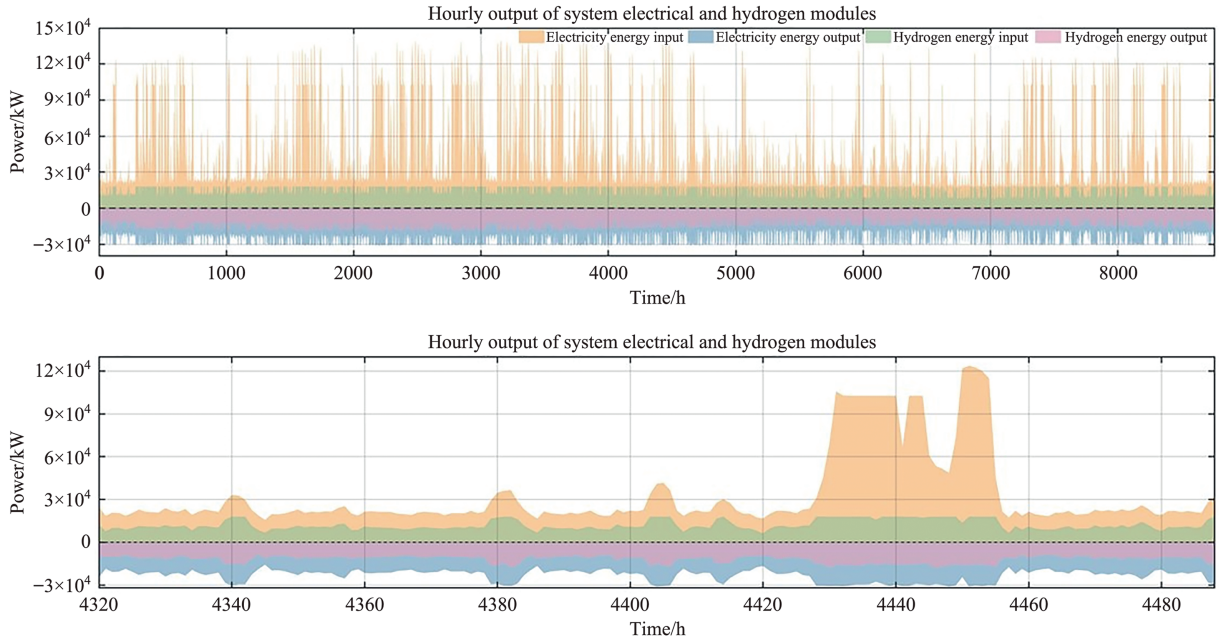


Fig. 9. Hourly energy output of the electricity-hydrogen module in a system with fuel cells integrated.

and stability. However, under heat demand, cooling demand, and renewable energy fluctuation uncertainties, SOFC integration fails to mitigate negative effects and exacerbates system costs.

Therefore, in the optimal design of energy systems, SOFCs should be reasonably configured based on the type and degree of uncertainty factors to fully leverage their advantages in the complementary conversion of electrical and hydrogen energy. At the same time, it is important to avoid the potential decrease in economic efficiency that they may bring in other scenarios, to achieve the optimal balance between cost and stability. These research findings provide significant decision support for the optimization of integrated energy systems in industrial parks and other similar areas.

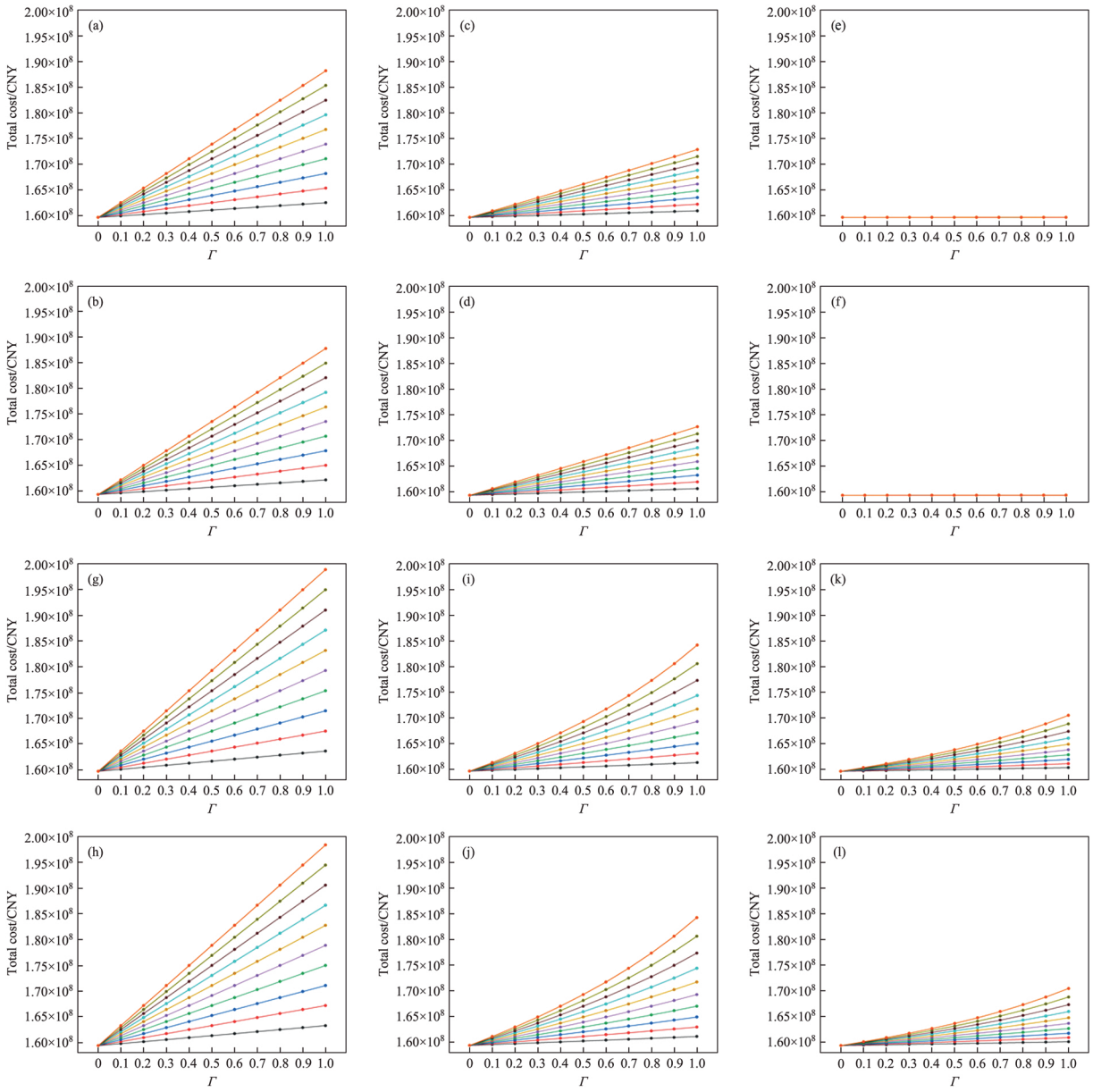


Fig. 10. The impact of uncertainty in multiple factors on the annual total cost of the system ((a), (b): Electricity demand uncertainty in systems without and with fuel cells; (c), (d): Heat demand uncertainty in systems without and with fuel cells; (e), (f): Cooling demand uncertainty in systems without and with fuel cells; (g), (h): Hydrogen demand uncertainty in systems without and with fuel cells; (i), (j): Wind power uncertainty in systems without and with fuel cells; (k), (l): PV power uncertainty in systems without and with fuel cells).

6. Conclusions

This study investigates the economic feasibility and system integration strategies of SOFCs in distributed IES. Through sensitivity analysis, optimal configuration, and uncertainty analysis, the application potential of SOFCs and their key influencing factors under different scenarios are systematically explored.

(1) The economic feasibility of SOFCs is jointly influenced by policy instruments, demand structure, and technological parameters. Higher carbon price levels and increased electricity and hydrogen demand significantly enhance the economic competitiveness of SOFCs, whereas rising thermal and cooling demand weakens their advantages, particularly under high thermal load conditions. Improvements in SOFC efficiency and service lifetime can effectively reduce system costs and enhance overall economic performance.

(2) SOFC integration delivers pronounced carbon mitigation benefits and improves renewable energy utilization. Specifically, system-wide CO_2 emissions are reduced by 7.8% following SOFC deployment. Moreover, by enabling flexible electricity–hydrogen conversion, SOFCs lead to a 7.1% reduction in electricity curtailment. These results highlight the strong potential of SOFCs in supporting decarbonization and improving renewable energy utilization.

(3) Uncertainty analysis indicates that hydrogen demand uncertainty has the greatest impact on system economics.

Under uncertainties in electricity and hydrogen demand, SOFCs effectively mitigate cost fluctuations and enhance operational stability through their flexible electricity–hydrogen conversion capability. Therefore, in the optimization and design of energy systems, it is necessary to comprehensively consider uncertainty factors and to configure SOFCs rationally to fully exploit their electricity–hydrogen conversion advantages.

CRediT Authorship Contribution Statement

Zihan Cheng: Writing – original draft, Validation, Methodology. Xiaojuan Ma: Software, Investigation. Yufei Wang: Writing – review & editing, Supervision, Conceptualization.

Declaration of Competing Interest

The authors declare that they have no known competing financial interests or personal relationships that could have appeared to influence the work reported in this paper.

Acknowledgements

Financial support by Beijing Natural Science Foundation (L259009) and Frontier Interdisciplinary Exploration Research Program of China University of Petroleum, Beijing (2462025XKQY002) is gratefully acknowledged.

Nomenclature

$\widehat{a}_t$	maximum deviation of uncertain parameters at time t, kW
B_f	if select the equipment f, $B_f = 1$
C_{emission}	the cost of carbon emission of the system, CNY·a^{-1}
C_{fuel}	fuel cost of the system, CNY·a^{-1}
C_i	cost of facility, CNY·a^{-1}
C_{Tot}	minimum total annual cost of the system, CNY·a^{-1}
C_f^{INV}	initial capital cost of equipment, CNY·kW^{-1}
$C_f^{\text{O\&M}}$	operation and maintenance cost of f, CNY·kW^{-1}·a^{-1}
$\text{CE}_{\text{emission}}$	carbon price, CNY·(t CO_2)$^{-1}$
CE_{gas}	price of natural gas, CNY·m^{-3}
COP_{ABC}	refrigeration coefficient of ABC
COP_{COC}	refrigeration coefficient of COC
$\overline{D}_t$	nominal value of energy demand at time t, kW
D_t^{cool}	the cooling energy demand of the system at time t, kW
D_t^{elec}	electricity demand of the system at time t, kW
D_t^{heat}	the thermal energy demand of the system at time t, kW
D_t^{hydrogen}	hydrogen demand of the system at time t, kg
EF_{gas}	CO_2 emissions per unit volume of natural gas, t CO_2·m^{-3}
F	set of all equipment in the energy system
f	specific equipment in the energy system
H_{CH_4}	the lower heating value of natural gas, kJ·m^{-3}
H_{H_2}	higher heating value of hydrogen, kJ·kg^{-1}
H^{Obs}	measurement height of the WT, m
H^{WT}	hub height of the WT, m
I_t^G	incident solar radiation on PV modules at time t, W·h·m^{-2}
$I^{\text{G,STC}}$	incident solar radiation on PV modules under standard test conditions, W·h·m^{-2}
i	depreciation rate of equipment, %
$N_{t,\text{CS}}^{\text{ch}}$	input power of CS at time t, kW
$N_{t,\text{BT}}^{\text{dis}}$	output power of BT at time t, kW
$N_{t,f}^{\text{dis}}$	output power of f at time t, kW
$N_{t,\text{CS}}^{\text{dis}}$	output power of CS at time t, kW
$N_{t,\text{HS}}^{\text{dis}}$	output power of HS at time t, kW
$N_{t,\text{HST}}^{\text{in}}$	input hydrogen quantity of the HST at time t, kg
$N_{t,\text{HST}}^{\text{out}}$	output hydrogen quantity of HST at time t, kg
NT	the total annual operating hours of the system, h
n_f	service life of equipment, a
n^{WT}	the total number of WTs, units
$P_{t,\text{ABC}}$	power input to the ABC at time t, kW
$P_{t,\text{ALK}}$	power input to the ALK at time t, kW
$P_{t,\text{COC}}$	power input to the COC at time t, kW
$P_{t,\text{DB}}$	power input to the DB at time t, kW
$P_{t,\text{FC}}$	power generated by the FC at time t, kW
$P_{t,f}$	energy input to equipment at time t, kW
$P_{t,\text{GT}}$	power input to the GT at time t, kW
$P_{t,\text{gas}}$	natural gas consumption at time t, m^3
$P_{t,\text{WB}}$	power input to the WB at time t, kW
$P_{t,\text{ALK}}^{\text{hydrogen}}$	hydrogen production by the ALK, kg·h^{-1}
$P_{t,\text{FC}}^{\text{hydrogen}}$	hydrogen input to the FC at time t, kg·h^{-1}
$P^{\text{PV,Rated}}$	the rated power of the PV system, kW
P_t^{PV}	power generated by the PV at time t, kW
$\overline{P}_t^{\text{PV}}$	nominal value of solar power generation at the time t, kW
$P_{t,1}$	dual variable of the standard optimization problem
P_t^{WT}	power generated of WT at time t, kW
$P_{t,j}^{\text{WT}}$	output power of a single WT at time t, kW
$\overline{P}_t^{\text{WT}}$	nominal value of wind power generation at the time t, kW
$P^{\text{WT,Rated}}$	rated power of a single WT, kW
$P^{\text{PV,Rated}}$	the rated power of the PV system, kW
R^{WT}	blade radius of the WT, m
$\text{SP}_{t,f}$	stored energy level of energy storage equipment at time t, kW·h
$\text{SP}_{t,\text{HST}}^{\text{hydrogen}}$	stored hydrogen level of the HST at time t, kg
T_t^{PV}	temperature of PV modules at time t, °C
$T^{\text{PV,STC}}$	temperature of PV modules under standard test conditions, °C
t	the unit time, h
$v^{\text{Cut-in}}$	cut-in wind speed of the WT, m·s^{-1}
$v^{\text{Cut-out}}$	cut-out wind speed of the WT, m·s^{-1}
v^{Rated}	rated wind speed of the WT, m·s^{-1}
v_t	the wind speed at the hub height of the WT, m·s^{-1}
v_t^{Obs}	wind speed at the measurement height, m·s^{-1}
W_f	rated capacity of f in the system
$W_{\max}$	maximum capacity of equipment
Z_t	dual variable of the standard optimization problem
z^0	surface roughness at the WT location, m
Γ	control parameter
$\eta^{\text{PV,Derating}}$	average degradation factor of PV modules
$\eta^{\text{PV,Derating,F}}$	degradation factor of PV modules in the first year of operation
$\eta^{\text{PV,Derating,A}}$	annual degradation factor of PV modules after the first year
η^{WT}	efficiency of an individual WT, %
$\eta^{\text{WT,System}}$	the overall efficiency of the wind power generation system, %
$\eta^{\text{PV,System}}$	operational efficiency of the PV system, %
$\eta_{\text{ALK,hydrogen}}$	hydrogen production efficiency of ALK, %
$\eta_{\text{DB,heat}}$	heat production efficiency of DB, %
$\eta_{\text{FC,elec}}$	power generation efficiency of FC, %
$\eta_{\text{FC,heat}}$	heat production efficiency of FC, %

$\eta_{GT,heat}$ heat production efficiency of GT, %
$\eta_{WB,heat}$ heat production efficiency of WB, %
$\eta_{DB,heat}$ heat production efficiency of DB, %
$\eta_{ALK,hydrogen}$ hydrogen production efficiency of ALK, %
η_f^{loss} energy loss coefficient of energy storage equipment, %
η_f^{ch} input efficiency of energy storage equipment, %
η_f^{dis} output efficiency of energy storage equipment, %
η_{HST}^{in} input efficiency of the HST, %
η_{HST}^{out} output efficiency of the HST, %
ρ^{Air} air density, $kg \cdot m^{-3}$
λ temperature coefficient of PV module power output
Φ utilization rate of natural gas, %
ϕ disturbance coefficient

References

[1] C. Ghenai, M. Albawab, M. Bettayeb, Sustainability indicators for renewable energy systems using multi-criteria decision-making model and extended SWARA/ARAS hybrid method, *Renew. Energy* 146 (2020) 580–597.
[2] L. Chen, G. Msigwa, M.Y. Yang, A.I. Osman, S. Fawzy, D.W. Rooney, P.S. Yap, Strategies to achieve a carbon neutral society: a review, *Environ. Chem. Lett.* 20 (4) (2022) 2277–2310.
[3] A. Kasaeian, E. Bellos, A. Shamaeizadeh, C. Tzivanidis, Solar-driven polygeneration systems: recent progress and outlook, *Appl. Energy* 264 (2020) 114764.
[4] X. Yao, B.W. Yi, Y. Yu, Y. Fan, L. Zhu, Economic analysis of grid integration of variable solar and wind power with conventional power system, *Appl. Energy* 264 (2020) 114706.
[5] M. Rezaei, K.R. Khalilpour, M.A. Mohamed, Co-production of electricity and hydrogen from wind: a comprehensive scenario-based techno-economic analysis, *Int. J. Hydrogen Energy* 46 (35) (2021) 18242–18256.
[6] B. Bhandari, K.T. Lee, C.S. Lee, C.K. Song, R.K. Maskey, S.H. Ahn, A novel off-grid hybrid power system comprised of solar photovoltaic, wind, and hydro energy sources, *Appl. Energy* 133 (2014) 236–242.
[7] M. Al-Nimr, S. Kiwan, H. Sharadga, A hybrid TEG/wind system using concentrated solar energy and chimney effect, *Int. J. Energy Res.* 42 (7) (2018) 2548–2563.
[8] X.S. Lü, T. Lu, S. Karirinne, A. Mäkiranta, D. Clements-Croome, Renewable energy resources and multi-energy hybrid systems for urban buildings in Nordic climate, *Energy Build.* 282 (2023) 112789.
[9] L. Ramirez Camargo, J. Valdes, Y. Masip Macia, W. Dorner, Assessment of on-site steady electricity generation from hybrid renewable energy systems in Chile, *Appl. Energy* 250 (2019) 1548–1558.
[10] T. Bin Nadeem, M. Siddiqui, M. Khalid, M. Asif, Distributed energy systems: a review of classification, technologies, applications, and policies, *Energy Strategy Rev.* 48 (2023) 101096.
[11] T.A. Nguyen, M. Mikami, Effect of hydrogen addition to intake air on combustion noise from a diesel engine, *Int. J. Hydrogen Energy* 38 (10) (2013) 4153–4162.
[12] J.D. Holladay, J. Hu, D.L. King, Y. Wang, An overview of hydrogen production technologies, *Catal. Today* 139 (4) (2009) 244–260.
[13] C.W. Forsberg, Future hydrogen markets for large-scale hydrogen production systems, *Int. J. Hydrogen Energy* 32 (4) (2007) 431–439.
[14] D. Jiang, Y. Jia, Q. Lu, B. Hong, R. Shen, Y. Zhang, Application prospect of hydrogen energy in integrated energy systems, *Electr. Power* 53 (5) (2020) 135–142.
[15] L.J. Ge, B.H. Zhang, W.T. Huang, Y.Z. Li, L.Y. Hou, J.B. Xiao, Z.M. Mao, X.P. Li, A review of hydrogen generation, storage, and applications in power system, *J. Energy Storage* 75 (2024) 109307.
[16] S. Bennoua, A. Le Duigou, M.M. Quéméré, S. Dautremont, Role of hydrogen in resolving electricity grid issues, *Int. J. Hydrogen Energy* 40 (23) (2015) 7231–7245.
[17] H.Q. Zhou, J.Y. Xue, H.B. Gao, N. Ma, Hydrogen-fueled gas turbines in future energy system, *Int. J. Hydrogen Energy* 64 (2024) 569–582.
[18] B.C. Tashie-Lewis, S.G. Nnabuife, Hydrogen production, distribution, storage and power conversion in a hydrogen economy - a technology review, *Chem. Eng. J. Adv.* 8 (2021) 100172.
[19] A.R. Razmi, A.R. Hanifi, M. Shahbakhti, Comparative techno-economic assessment of solid oxide fuel cells versus hydrogen-fueled internal combustion engines for institutional energy management, *Fuel* 405 (2026) 136680.
[20] L.X. Fan, Z.K. Tu, S.H. Chan, Recent development of hydrogen and fuel cell technologies: a review, *Energy Rep.* 7 (2021) 8421–8446.
[21] J. Lindorfer, D.C. Rosenfeld, H. Böhm, Fuel cells, Future Energy, Elsevier, 2020, pp. 95–517.
[22] J. Hosseinpour, A. Chitsaz, L. Liu, Y. Gao, Simulation of eco-friendly and affordable energy production *via* solid oxide fuel cell integrated with biomass gasification plant using various gasification agents, *Renew. Energy* 145 (2020) 757–771.
[23] A.R. Razmi, S. Sharifi, S. Vafaeenezhad, A.R. Hanifi, M. Shahbakhti, Modeling and microstructural study of anode-supported solid oxide fuel cells: experimental and thermodynamic analyses, *Int. J. Hydrogen Energy* 54 (2024) 613–634.
[24] A.B.M. Ali, A.K. Nemah, Y.A. Al Bahadli, E. Kianfar, Principles and performance and types, advantages and disadvantages of fuel cells: a review, *Case Stud. Chem. Environ. Eng.* 10 (2024) 100920.
[25] D. Das, R. Esmaili, L. Xu, D. Nichols, An optimal design of a grid connected hybrid wind/photovoltaic/fuel cell system for distributed energy production, in: 31st Annual Conference of IEEE Industrial Electronics Society, IEEE, Raleigh, NC, USA, 2006.
[26] T.F. El-Shatter, M.N. Eskander, M.T. El-Hagry, Energy flow and management of a hybrid wind/PV/fuel cell generation system, *Energy Convers. Manag.* 47 (9–10) (2006) 1264–1280.
[27] L. Sun, Y.H. Jin, L. Pan, J. Shen, K.Y. Lee, Efficiency analysis and control of a grid-connected PEM fuel cell in distributed generation, *Energy Convers. Manag.* 195 (2019) 587–596.
[28] L. Sun, Y.H. Jin, J. Shen, F.Q. You, Sustainable residential micro-cogeneration system based on a fuel cell using dynamic programming-based economic day-ahead scheduling, *ACS Sustainable Chem. Eng.* 9 (8) (2021) 3258–3266.
[29] L. Li, B.L. Dou, H. Zhang, L. Zhang, N. Chen, H.S. Chen, Y.J. Xu, W. Li, Design, modelling and experimental validation of integrated hydrogen-ammonia-methanol multi-carrier energy conversion for the emerging solid oxide fuel cell with waste heat recovery technology, *Energy* 335 (2025) 137927.
[30] I. Sebbani, M.K. Ettouhami, M. Boulakhbar, Fuel cells: a technical, environmental, and economic outlook, *Clean. Energy Syst.* 10 (2025) 100168.
[31] D.B. Nelson, M.H. Nehrir, C. Wang, Unit sizing of stand-alone hybrid wind/PV/fuel cell power generation systems, in: IEEE Power Engineering Society General Meeting, IEEE, San Francisco, CA, USA, 2005, pp. 2116–2122.
[32] A. Maleki, F. Pourfayaz, Sizing of stand-alone photovoltaic/wind/diesel system with battery and fuel cell storage devices by harmony search algorithm, *J. Energy Storage* 2 (2015) 30–42.
[33] Y.T. Yang, Y.L. Shen, T.L. Sun, P. Liu, T.Z. Lei, Economic analysis of solid oxide fuel cell systems utilizing natural gas as fuel, *Energies* 17 (11) (2024) 16.
[34] C.A. Gibson, M.A. Meybodi, M. Behnia, A methodology to compare the economic feasibility of fuel cell-, gas turbine- and microturbine-based combined heat and power systems, *Int. J. Energy Res.* 40 (7) (2016) 983–1008.
[35] M. Wang, Z.P. Shi, W. Luo, Y. Sui, D.X. Wu, Distributionally robust optimal scheduling of integrated energy systems including hydrogen fuel cells considering uncertainties, *Energy Rep.* 10 (2023) 1575–1588.
[36] Z.J. Lu, Q. Zhu, W.G. Zhang, H.J. Lin, Economic operation strategy of integrated hydrogen energy system considering the uncertainty of PV power output, *Energy Rep.* 9 (2023) 463–471.
[37] S. Rajper, I.J. Amin, Optimization of wind turbine micrositing: a comparative study, *Renew. Sustain. Energy Rev.* 16 (8) (2012) 5485–5492.
[38] Wind Characteristics and Resources, Wind Energy Explained, 2009.
[39] F. Ali, M. Ahmar, Y.X. Jiang, M. AlAhmad, A techno-economic assessment of hybrid energy systems in rural Pakistan, *Energy* 215 (2021) 119103.
[40] D. Bertsimas, M. Sim, Robust discrete optimization and network flows, *Math. Program.* 98 (1) (2003) 49–71.
[41] Q. Zhang, H.R. Zhang, Y.M. Yan, J. Yan, J.J. He, Z.B. Li, W.L. Shang, Y.T. Liang, Sustainable and clean oilfield development: how access to wind power can make offshore platforms more sustainable with production stability, *J. Clean. Prod.* 294 (2021) 126225.
[42] Z.Y. Cui, Y. Wu, S.B. Chen, S.Y. Bian, S. Tang, Y.F. Wang, C.M. Xu, Generalized methodology for the optimization of biomass-green hydrogen-based e-fuel system, *Appl. Energy* 378 (2025) 124819.
[43] F. Rosner, A. Rao, S. Samuelsen, Economics of cell design and thermal management in solid oxide fuel cells under SOFC-GT hybrid operating conditions, *Energy Convers. Manag.* 220 (2020) 112952.
[44] P. Marocco, M. Gandiglio, M. Santarelli, When SOFC-based cogeneration systems become convenient? A cost-optimal analysis, *Energy Rep.* 8 (2022) 8709–8721.
[45] D.C. Li, H.L. Yang, Economic feasibility of LNG-fuelled river ships: carbon tax schemes perspective, *Transp. Res., Part D Transp. Environ.* 132 (2024) 104235.